Earth and Planetary Science Letters 383 (2013) 82–91

Contents lists available at ScienceDirect

Earth and Planetary Science Letters

www.elsevier.com/locate/epsl

The fidelity of paleomagnetic records carried by magnetosome chains

Greig A. Paterson *, Yinzhao Wang, Yongxin Pan

Paleomagnetism & Geochronology Laboratory, Key Laboratory of Earth's Deep Interior, Institute of Geology and Geophysics, Chinese Academy of Sciences, Beijing 10029, China

ARTICLE INFO

Article history:
Received 30 May 2013
Received in revised form 19 September 2013
Accepted 20 September 2013
Available online xxxx
Editor: J. Lynch-Stieglitz

Keywords:
magnetotactic bacteria
sedimentary magnetism
relative paleointensity
magnetofossils
magnetic interactions

ABSTRACT

Magnetotactic bacteria (MTB), which use aligned chains of magnetosomes (magnetic crystals) as a navigation tool, are found in a wide range of modern day marine, river and lacustrine environments and their fossilized remains are being increasing recognized in geological records. Despite an increasing realization that biogenically derived magnetic particles may play a key role in sedimentary magnetizations, little is known about the influence that they may have on the fidelity of paleomagnetic recordings. Using cultured *Magnetospirillum magneticum* strain AMB-1, we have conducted simple 2D (i.e., zero-inclination) deposition experiments to assess the efficiency with which magnetosome chains align along magnetic field lines and the implications that this has for paleomagnetic records. Our results indicate that the natural remanent magnetization (NRM) acquired by deposited MTB is near linear with applied field (0–120 μT), but that NRM acquisition does not perfectly follow the assumed linear trend and over a six-fold increase in applied field only a factor ~5.5 increase in NRM intensity is observed (i.e., ~9% lower than the assumed trend). Both anhysteretic remanent magnetization (ARM) and saturation isothermal remanent magnetization (SIRM) normalized relative paleointensities (RPIs) can successfully recover field strength variations under identical situations. When the MTB concentration of the initial solution is varied (up to a factor 8), NRM carried by MTB responds in the expected fashion (i.e., a doubling of bacteria produces a doubling of NRM intensity). Both ARM and SIRM, however, do not respond to as expected: A doubling of concentration corresponds to an increase of ~1.76 in SIRM intensity and an increase of only ~1.63 in ARM intensity. Both are influenced by magnetostatic interactions that arise from the close packing of bacterial cells or subchain interactions within a single bacterial cell. First-order reversal curve (FORC) diagrams, however, are too insensitive to indicate the presence of paleomagnetically relevant magnetic interactions. Remanence based methods (i.e., the ARM ratio) are more appropriate to detect such interactions.

1. Introduction

Paleo- and rock magnetic records obtained from marine and lake sediments are a vital tool for high resolution reconstructions of paleomagnetic field behaviour (e.g., Guyodo and Valet, 1996; Korte and Constable, 2005) and for paleoclimatic proxies (e.g., Larrasoaña et al., 2008). It is therefore important to test the fidelity of such magnetic records to provide better constraints on the paleo-Earth. It is increasingly being recognized that magnetotactic bacteria (MTB), which are prokaryotes that use biomineralized chains of magnetic crystals (magnetite or greigite) to navigate by geomagnetic field lines (Frankel and Blakemore, 1980; Bazylinski and Frankel, 2004), may play a significant role in the magnetization of sediments from a wide range of environments (e.g., Kirschvink, 1982; Petersen et al., 1986; Stolz et al., 1986; Chang et al., 1987; Tarduno et al., 1998; Egli, 2004; Pan et al., 2005; Kopp and Kirschvink, 2008; Roberts et al., 2011, 2012; Lin et al., 2012). How well MTB can record the paleomagnetic field, however, has yet to be tested and recent inferences made from geological records suggest that the mechanism by which MTB may acquire a magnetization in sediments may violate assumptions made about sedimentary magnetizations (Roberts et al., 2012; Yamazaki et al., 2013).

The inter-cellular magnetic particles that MTB biomineralize, known as magnetosomes, typical fall within the single domain (SD) magnetic grain size range and are spatially arranged in chains, which make them the optimal size for navigation purposes (Hanzlik et al., 1996; Muxworthy and Williams, 2006, 2009). Most individual magnetosomes are ~35–120 nm in size; however, empirical data supporting the validity of relative paleointensity (RPI) records from sediments is restricted to grain sizes on the order of 1–15 μm (King et al., 1983; Tauxe, 1993) and the influence of the chain structure on RPI estimates remains unquantified. Anhysteretic remanent magnetization (ARM), which is widely used to normalize RPI records, is sensitive to SD grains and should therefore be sensitive to magnetosomes. This has led to the suggestion

* Corresponding author.
E-mail address: greig.paterson@mail.iggcas.ac.cn (G.A. Paterson).

0012-821X/$ – see front matter
http://dx.doi.org/10.1016/j.epsl.2013.09.031

that changes in the relative abundance of MTB derived magnetic particles with respect to detrital magnetic grains may cause large biases in ARM and hence bias ARM normalized RPI (Roberts et al., 2012). To-date, however, no laboratory control experiments have been conducted to test the fidelity of paleomagnetic records carried by MTB.

In this study, we have undertaken simple 2D (i.e., zero-inclination) deposition experiments using intact MTB cells. These experiments have been used to investigate the first-order characteristics of how intact MTB record the ambient magnetic field, which includes the linearity of magnetization with applied field, the effects of remanence anisotropy, and the behaviour and fidelity of relative paleointensity estimates.

2. Methods

2.1. Sample preparation

Magnetospirillum magneticum AMB-1 (ATCC strain 700264) were cultured using a modified ATCC-recommended medium at 26 °C and under aerobic static conditions. Bacterial cells were grown to the stationary growth phase and were concentrated by centrifugation at 10,000 rpm at 4 °C for ~10 min to produce bacterial solutions with concentrations of 10^{10}–10^{11} cells/mL.

2.2. Microscopy observations

Transmission election microscope (TEM) observations were made using a JEOL JEM-1400 with an accelerating voltage of 80 kV. Samples were prepared by washing the bacterial solution to remove residual salts from the culture medium. The solution was diluted and 20 µL was deposited onto carbon coated copper grids and allowed to air dry. The grids were washed two times by double distilled sterile water.

2.3. Magnetic measurements

Two milliliters of culture solution concentrated with AMB-1 cells were gently injected into standard paleomagnetic cubes by pipette. Solution mixing and the fluid motion during injection were sufficient to mix and randomize the orientation of the cells and hence the magnetosome chains. The cubes were placed within two orthogonal Helmholtz coils and allowed to settle and dry in an applied field over a period of 5–6 days. After drying, the MTB form thin layers in the base of the cubes. To prevent disturbance during measurement, the bacteria were glued in place; setting of the glue took place within the applied field. During the drying and setting process the samples were covered to prevent dust contamination.

The two Helmholtz coils were separately adjustable and were oriented such as to cancel the vertical component of the ambient magnetic field and adjust the horizontal component. The total field vector was restricted to the horizontal plane to avoid any potential influence of inclination shallowing. Deposition in 7 field strengths (B_{NRM}) was investigated: ~0, 20, 40, 60, 80, 100, and 120 µT. The zero-field deposition was conducted inside a magnetically shielded room (measured ambient fields $\leqslant$150–200 nT). Over the course of the experiments the average field for each experiment was maintained to within $\leqslant$0.22 µT of the desired field (typically $\leqslant$ 0.1 µT) and with an average vertical component $\leqslant$1.4% of the horizontal component (typically $\leqslant$0.5%).

For the non-zero fields, the measurements axes of the samples were placed in four orientations (0, 30, 60 and 90°) with respect to the applied field direction to allow the effects of orientation to be investigated. For each orientation three samples were used; a total of 75 samples were prepared. Due to weak natural remanent magnetizations (NRMs) from the zero-field experiments, the magnetizations of the empty paleomagnetic cubes were subtracted from the NRM measurements; this was not need for the in-field samples.

The effects of varying the MTB concentration of the initial solution on NRM acquisition and rock magnetic properties of the dried samples was investigated using diluted MTB solutions. Dilution was performed by diluting 0.25, 0.5, 1, and 2 mL of the same MTB solution with double distilled sterile water to produce a final solution volume of 2 mL. The effects of concentration were investigated using two B_{NRM} field strengths (40 and 100 µT) and with 2 replicate samples for averaging at each concentration. The applied laboratory field directions for all concentration samples were parallel to B_{NRM}. The initial bacterial solutions represent concentration variations, but the final volume of the dried samples could not be measured. Therefore the final samples are more representative of variations in the number of bacterial cells (i.e., a proxy for the amount of magnetizable material) rather than exact variations in final concentration. For simplicity, however, we describe our results in terms of the concentration of the initial solution, which can be viewed as the relative variation in the number of bacterial cells.

Magnetic remanence measurements were conducted on a 2G Enterprises 760 SQUID magnetometer housed within a shielded room. Alternating field (AF) demagnetization was carried out in 11–12 steps up to a peak field of 80–100 mT using the inline static AF demagnetizer of the magnetometer. Analysis of the NRM directions was performed using principal component analysis (PCA) following Kirschvink (1980). Following NRM demagnetization, anhysteretic remanent magnetization (ARM) was imparted using the magnetometer's inline coils with a bias field of 60 µT and a peak AF of 80 mT. Saturation isothermal remanent magnetization (SIRM) was imparted using an offline 2G Enterprises pulse magnetizer with a peak field of 1 T. Both ARM and SIRM were AF demagnetized using the above described steps. The anisotropy tensor of ARM and SIRM was determined by measuring magnetizations in 6 positions ($\pm x$, $\pm y$, and $\pm z$). After each magnetization acquisition the samples were demagnetized to determine a baseline. The anisotropy tensors were calculated following Tauxe (2010). IRM acquisition and back-field demagnetization was performed on the 2G pulse magnetizer using 15 steps up to a peak field of 300 mT.

Magnetic hysteresis, IRM acquisition, back-field demagnetization and first-order reversal curves (FORCs; Pike et al., 1999; Roberts et al., 2000) were measured on a Princeton Measurements Corporation vibrating sample magnetometer (model 3900). The FORCs were measured using 150 individual curves ($\delta B =$ 0.876 mT). The FORC diagrams were produced using the FORCme software of Heslop and Roberts (2012), which is based on the processing algorithm of Harrison and Feinberg (2008). For samples that had low signal-to-noise ratios, multiple FORC measurements were repeated and stacked to improve the quality of the data. All diagrams are produced using a smoothing factor (SF) of 3. The effective resolution for all FORC diagrams ($\Delta B = \delta B \times (SF + 1/2)$) is therefore $\Delta B = 3.1$ mT (Egli et al., 2010).

All rock and paleomagnetic measurement data are available for download through the MagIC database (http://earthref.org/MAGIC/).

3. Results

3.1. TEM observations

Example TEM observations are shown in Fig. 1. Each bacterial cell contains magnetosome chains in a fragmental configuration (Li et al., 2009) with 1–4 subchains per cell with each subchain consisting of 4–15 magnetite magnetosomes (average

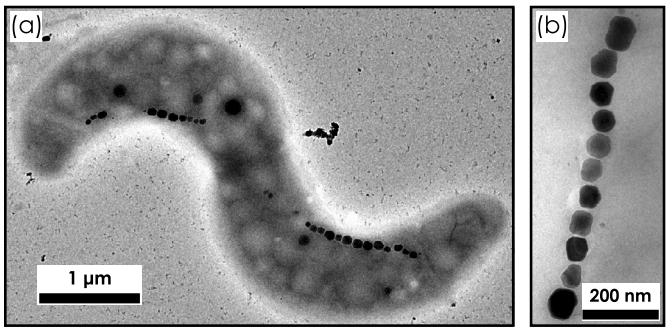

Fig. 1. TEM observations of (a) a typical AMB-1 bacterial cell and (b) a typical magnetosome chain.

of ~7). Subchains within a single cell are separated by an average distance of ~334 nm. Cell morphology and chain arrangement were not deformed. The average magnetosome size and shape factor (width/length), as deduced from 2D TEM observations, are 52.2 ± 13.5 nm and 0.85 ± 0.16, respectively (quoted errors are $\pm 1\sigma$, $N = 118$). The magnetosomes are approximately equidimensional crystals of SD magnetite.

3.2. Rock magnetic characteristics

The magnetic properties of our AMB-1 culture are shown in Fig. 2. This sample was prepared by concentrating the MTB solution and air drying the concentrate into a ~6 mm gelatin capsule. The cells were unoriented. This is the standard preparation method for cultured and extracted uncultured MTB that are widely used to infer rock magnetic behaviour of MTB (e.g., Li et al., 2009; Lin and Pan, 2009). The high-field properties are typical of MTB. The hysteresis loop (Fig. 2a) has a remanence ratio of 0.46 and a coercivity of 22.5 mT, which indicates SD behaviour. The crossover of the IRM acquisition and back-field demagnetization occurs at a normalized intensity of 0.496 (Fig. 2b), which indicates that the SD particles are non-interacting (Cisowski, 1981). The FORC diagram (Fig. 2c) further confirms these findings. The diagram exhibits a broad coercivity distribution with a peak at 33.5 mT and a narrow spread on the vertical axis. This is typical of non-interacting uniaxial SD particles and is characteristic of MTB with intact magnetosome chains and AMB-1 (e.g., Li et al., 2009; Egli et al., 2010).

3.3. Fidelity of the NRM

The NRMs of 5 samples (at B_{NRM}/angle combinations of 20 μT/0°, 20 μT/60°, 80 μT/30°, 100 μT/0°, and 100 μT/90°) were unstable during demagnetization and failed to yield acceptable data (e.g., unstable directions), which was likely due to disturbance during the sample drying period. These samples were excluded from further analysis.

PCA line fitting was used on the 10–50 mT AF demagnetization steps for all samples (8 data points). The maximum angular deviation (*MAD*) values are consistently below 5°, typically <3°, which indicates highly stable NRM directional demagnetization behaviour. As would be expected, all inclinations are shallow (−4.1–3.8°). Excluding the zero-field samples, the recorded declinations lie close to the expected values (Fig. 3a), with a small amount of scatter that can be accounted for by measurement errors and imprecision in sample orientation.

The dependence of NRM on B_{NRM} is shown in Fig. 3b. The NRM intensities range from 0.16–17.9 μAm^2. With the exception of the zero-field results, where the relative scatter is ~37% of the mean value, the scatter of the NRM intensities for each B_{NRM} is generally low (⩽7.6%). This suggests that the initial solution concentration is reasonably homogeneous for these samples. In Fig. 3b the NRM intensity data are fitted to a linear model, where it assumes that at

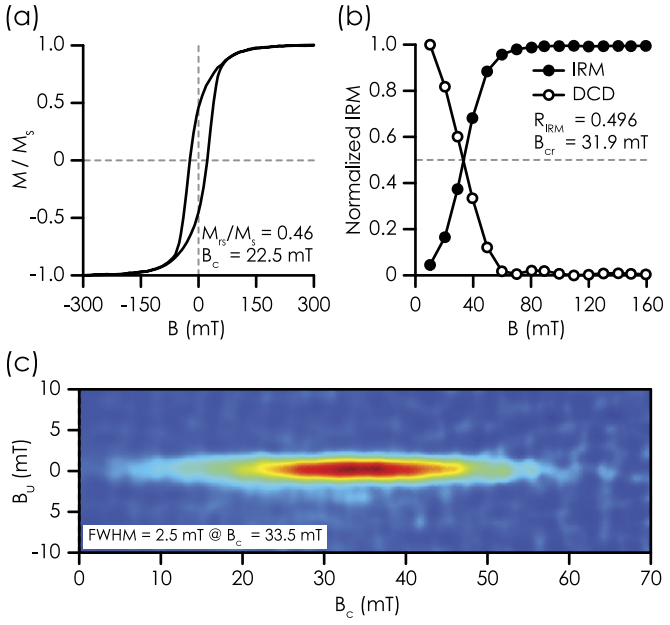

Fig. 2. Rock magnetic properties of the cultured AMB-1 MTB prepared in a gelatin capsule. (a) Hysteresis loop, (b) IRM acquisition and back-field demagnetization, and (c) FORC diagram. The FORC diagram was processed with FORCme (Heslop and Roberts, 2012) using a smoothing factor of 3 ($\Delta B = 3.1$ mT) and is the average of two FORC diagram measurements.

$B_{NRM} = 0$ zero magnetization is acquired (for our zero-field samples we measure a finite magnetization due to the cubes and the limits of equipment sensitivity). The 95% confidence interval for the fit was determined using a bootstrap approach (Efron, 1979) with 10^4 bootstraps. The individual measurements and not the average values are bootstrapped. As B_{NRM} increases the measured NRM underestimates the expected linear trend (dashed line in Fig. 3b; determined by scaling the $B_{NRM} = 20$ μT results). This expected relative linear trend is what we would expect if a two-fold increase in B_{NRM} resulted in a two-fold increase in the NRM intensity. By $B_{NRM} = 120$ μT (a six-fold increase) the measure NRM is ~9% less than the expected value from six times scaling of the 20 μT results. For most practical purposes, however, this difference is small.

3.4. ARM, SIRM, and relative paleointensities

Both ARM and SIRM are independent of the magnitude of B_{NRM}. The mean ARM and SIRM from the 70 measured samples are 8.6 ± 0.5 μAm^2 and 247.9 ± 40.5 μAm^2, respectively. The relative scatters are low (5.6% and 16.3%, respectively), but indicate that the SIRM measurements are noisier than the ARM measurements. The ARM ratio (χ_{ARM}/SIRM) for these samples is 0.74 ± 0.09 mmA^{-1}.

3.4.1. Remanence anisotropy

The angular dependence of ARM and SIRM is shown in Figs. 4a and 4b, respectively. If anisotropy has a significant influence on the laboratory magnetizations it should be expected that for angles close to 0° the laboratory remanence is acquired close to parallel to the magnetosome chain length (a magnetic easy axis), which should lie close the NRM acquisition field. Conversely, at angles close to 90°, the laboratory field should be applied close to perpendicular to the chain axis and hence close to the magnetic hard axis. Neither ARM nor SIRM exhibit a systematic trend with laboratory field angle (Fig. 4a and b). The principal axes of the 3D ARM anisotropy tensors for samples with $B_{NRM} \geqslant 40$ μT is shown in Fig. 4c and the mean axis directions and bootstrapped confidence intervals (Tauxe et al., 1998) are given in Fig. 4d. In these

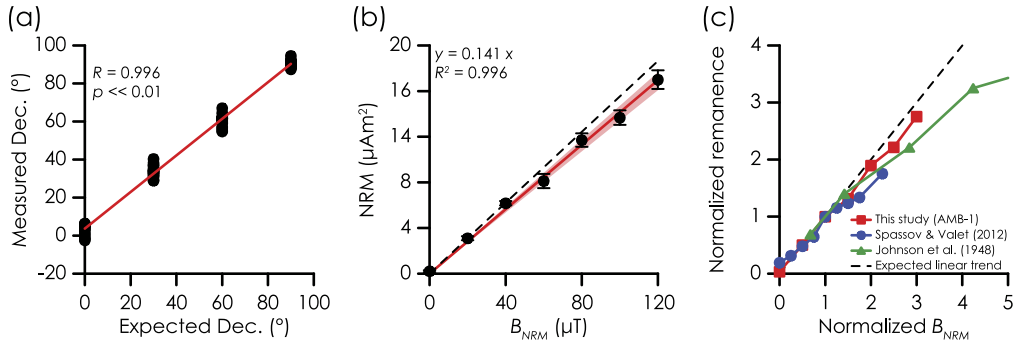

Fig. 3. (a) The measured magnetic declination as a function of the expected value. R is the Pearson linear correlation and p is the significance of the correlation. (b) The linearity of NRM with applied field (B_{NRM}) fitted using a linear model. The circles represent the averages of the measured data and the error bars are ± one standard deviation. The solid line is the linear model fit, the shaded area is the 95% confidence interval for the fit determined using a bootstrap approach, and the dashed line is the linear trend predicted by scaling the 20 μT mean result. R^2 is the coefficient of determination for the linear fit. (c) NRM acquisition with applied field for redeposited sediments (Johnson et al., 1948; Spassov and Valet, 2012) and MTB (this study). The NRM and B_{NRM} have been normalized by the 40 μT values for ease of comparison.

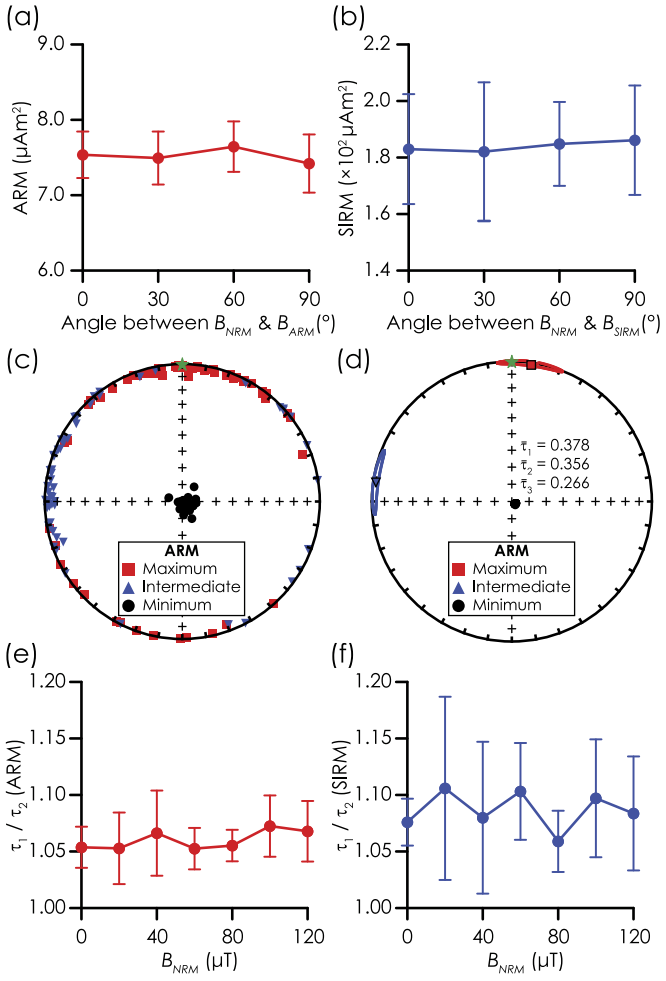

Fig. 4. The angular dependence of (a) ARM and (b) SIRM (the zero-field data are excluded). (c) The orientation of the principal anisotropy axes for ARM from samples with $B_{NRM} \geqslant 40$ μT. (d) The average ARM principal anisotropy axes and bootstrapped confidence intervals. The $\bar{\tau}$ values are the average eigenvalues of the principal anisotropy axes. The green stars in c and d represent the direction of B_{NRM}. The ratio of the maximum and intermediate eigenvalues for (e) ARM and (f) SIRM. In a, b, e and f, the circles represent the average values and the error bars are ± one standard deviation. (For interpretation of the references to color in this figure legend, the reader is referred to the web version of this article.)

figures the data have been rotated such that the x-axis of all samples has zero declination with respect to the applied field direction. As would be expected from a shallow deposition environment

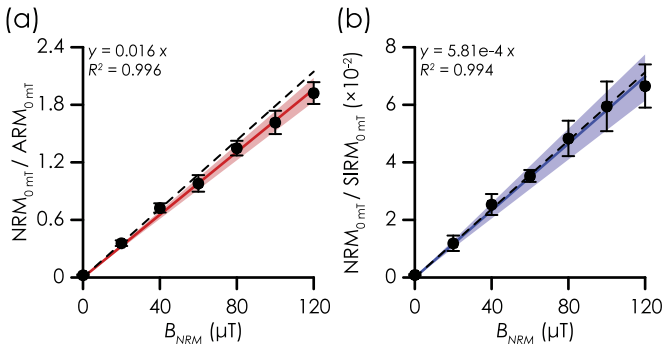

Fig. 5. The linearity of relative paleointensity estimates with applied field (B_{NRM}) when normalized by (a) ARM and (b) SIRM. The symbols are the same as in Fig. 3b.

and horizontal B_{NRM}, the minimum anisotropy axis is perpendicular to the deposition plane and the maximum and intermediate axes lie within the horizontal plane ($\bar{\tau}_1 \approx \bar{\tau}_2 > \bar{\tau}_3$). In general, the maximum principal axis lies along the direction of B_{NRM}, but is scattered with some intermediate axes lying close to the field direction Fig. 4c. The average degree of anisotropy (τ_1/τ_3) is high (~1.41 for ARM and ~1.35 for SIRM), which would be expected given a horizontal B_{NRM} and the potential inclination shallowing caused by the base of the cubes. The ratio of eigenvalues of the maximum and intermediate axes (τ_1 and τ_2, respectively) for the ARM and SIRM anisotropy tensors are shown in Figs. 4e and 4f, respectively. This ratio represents the anisotropy in the horizontal plane. For ARM, the average τ_1/τ_2 is ~1.06, but ranges from 1.01 to 1.16. For, SIRM τ_1/τ_2 ranges from 1.01 to 1.31 with an average value of ~1.09, this wider range of values is likely to be partially related to generally higher scatter associated with SIRM measurements. In general, $\tau_1 \approx \tau_2$ and in both cases there is no significant relation with the strength of B_{NRM}. Anisotropy is sufficient to produce an increased alignment of magnetosomes chains and thus produce larger NRM intensities for higher field strengths, and it is large enough for the principal ARM anisotropy axes to generally lie close to the direction of B_{NRM}; however, anisotropy appears to be insufficient to greatly influence the normalizers used for RPI estimates.

3.4.2. Relative paleointensity

ARM and SIRM normalized paleointensities as a function of B_{NRM} are shown in Fig. 5. In both cases the data have been fitted with a linear model as described for the NRM. For both ARM and SIRM normalized RPI the average values follow a linear trend. The linear trend of the ARM normalized RPI, however, varies slightly

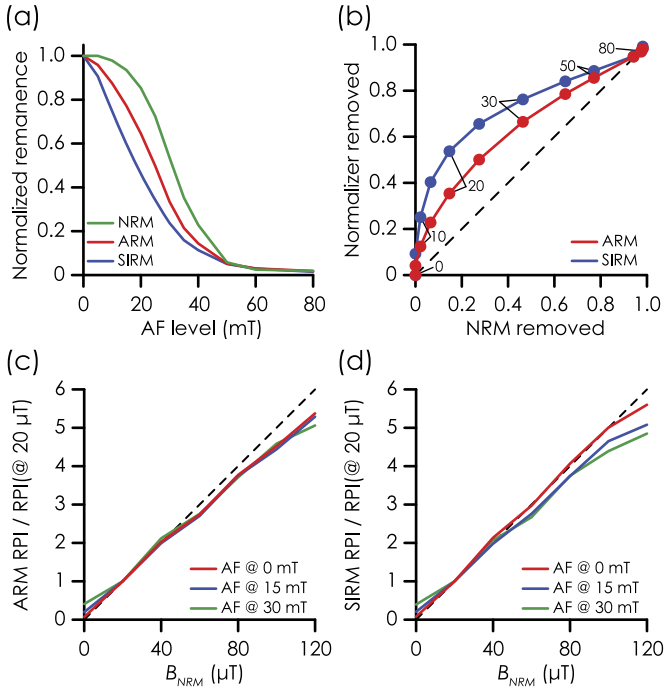

Fig. 6. (a) Average AF demagnetization behaviour of normalized NRM, ARM, and SIRM. (b) Average ARM and SIRM demagnetization plotted against average NRM demagnetization. The dashed line represents the desired one-to-one ratio. Numbers denote the AF demagnetization level in mT. (c) ARM and (d) IRM relative paleointensities after varying levels of AF demagnetization.

from the expected relative trend. At $B_{NRM} = 120$ μT the measured RPI underestimates this expected trend by ~10%. That is to say, for a six-fold increase in B_{NRM}, ARM normalized RPI only increases by a factor of ~5.4. The similarity of ARM normalized RPI and NRM acquisition indicates that ARM RPI is representative of the NRM behaviour. For the SIRM normalized RPI estimates the data appear to fall close to the expected trend (i.e., a doubling in field intensity yields a doubling of magnetization). It should be noted, however, that the scatter of the data and hence the 95% confidence interval of the fit is larger for SIRM than for ARM. This higher degree of scatter of the SIRM measurements (16.3% of the mean value, compared to 5.6% for the ARM) is likely to be partially obscuring the deviation of the NRM intensity from the expected trend.

3.4.3. Demagnetization behaviour

The average AF demagnetization behaviour of NRM, ARM, and SIRM are shown in Fig. 6a. The remanence demagnetization behaviour of all samples is highly consistent and the normalized averages shown in this figure are representative of typical demagnetization behaviour. The behaviour of the three magnetizations is distinct with NRM being the most magnetically hard, ARM is softer, and SIRM is the softest. The average median destructive field (MDF) of the NRM is 31.0 ± 0.8 mT ($\pm 1\sigma$). For ARM and SIRM the average MDF values are 24.9 ± 0.7 mT and 18.5 ± 1.4 mT, respectively. When plotted as ARM or SIRM lost against NRM lost, as in Fig. 6b, the non-linear relationship between NRM and ARM or SIRM coercivity spectra can be clearly seen. This suggests that the choice of AF level used to remove any overprints may influence the RPI determination. This is explored for ARM (Fig. 6c) and SIRM (Fig. 6d) after 0, 15, and 30 mT AF demagnetization. In these figures the RPI estimates have been normalized by the values from the $B_{NRM} = 20$ μT experiments. Since the ARM coercivity spectra are most similar to the NRM spectra, the RPI estimates are least affected by the level of AF demagnetization. At 0 mT AF, the 120 μT ARM RPI underestimates the expected trend by ~10%, but this increases to ~16% by 30 mT AF. The effects for SIRM are more pronounced due to the larger difference in coercivity spectra (Fig. 6a and b) and by 30 mT AF the 120 μT RPI values underestimate the expected trend by ~19% (Fig. 6d). If a pseudo-Thellier approach (Tauxe et al., 1995) were to be used to estimate RPI, the estimate would be highly dependent on the choice of AF demagnetization levels used for the best-fit linear segment. As can be seen in Fig. 6b, however, the difference in coercivity spectra of the NRM and laboratory magnetizations would produce highly curved pseudo-Arai plots, which would typically be rejected by this method.

3.5. The effects of increasing cell concentration in the initial solution

For the $B_{NRM} = 40$ μT experiments, the average NRM intensities range from 8.9–48.5 μAm^2, ARM from 12.8–34.9 μAm^2, and SIRM from 243.2–915.9 μAm^2. For the $B_{NRM} = 100$ μT experiments, average NRM values range from 9.3–109.0 μAm^2, ARM from 8.9–39.4 μAm^2, and SIRM from 204.0–870.2 μAm^2. Due to differences in the concentration process, the magnetizations of the samples with 2 mL of bacterial solution from the second culture of MTB are approximately 8 times higher than those from the first culture, which indicates a ~8 times higher concentration.

The average remanent magnetizations as a function of initial solution concentration are shown in Fig. 7a–c. In this figure the magnetizations have been normalized by the average magnetization from the 1 mL concentration samples, which allows the relative scaling of magnetization with concentration to be easily compared for the two fields. For the investigated field strengths, the NRM is linearly proportional to the concentration of MTB in the initial solution and the slopes of the best linear fits for both fields (0.992 and 1.097, for $B_{NRM} = 40$ μT and 100 μT, respectively) are close to the expected trend (a slope of unity). This indicates that the magnetic particles in all samples respond in the same manner to B_{NRM} (i.e., a two-fold increase in the number of bacterial cells produces a two-fold increase in magnetization).

The intensity of ARM and SIRM appear to increase near linearly with solution concentration, but deviate from the expected trends. For ARM, a two-fold increase in the initial solution concentration only corresponds to a ~1.5–1.7 times increase in ARM intensity. For SIRM, a doubling of the solution concentration yields a ~1.7–1.8 times increase in SIRM intensity. Although near linear, the fact the ARM and SIRM trends do not tend towards the origin (i.e., zero magnetization for zero MTB) indicates that the trends are non-linear, which is an indication that these data are influenced by magnetic interactions (e.g., Egli, 2006).

For each B_{NRM} the RPI is expected to be constant. That is to say, if laboratory magnetizations are suitable proxies for variations in the number of bacteria, RPI should be independent of the solution concentration. ARM and SIRM normalized RPIs are shown in Figs. 7d and 7e, respectively. As before, the values have been normalized by the 1 mL concentration values and all RPIs are expected to be unity. The 0.25 mL samples for the 100 μT RPI results give anomalously low values, which is likely due to heterogeneity in the number of MTB cells in these samples where only two samples are insufficient for averaging. For both ARM and SIRM normalization it can be clearly seen that RPI is dependent on the solution concentration. The effect is most pronounced for ARM due it being a poorer proxy at high solution concentrations.

4. Discussion

4.1. The role and manifestation of magnetic interactions

Based on the less than expected increase of ARM and SIRM intensity with number of bacteria, the indication of a non-linear

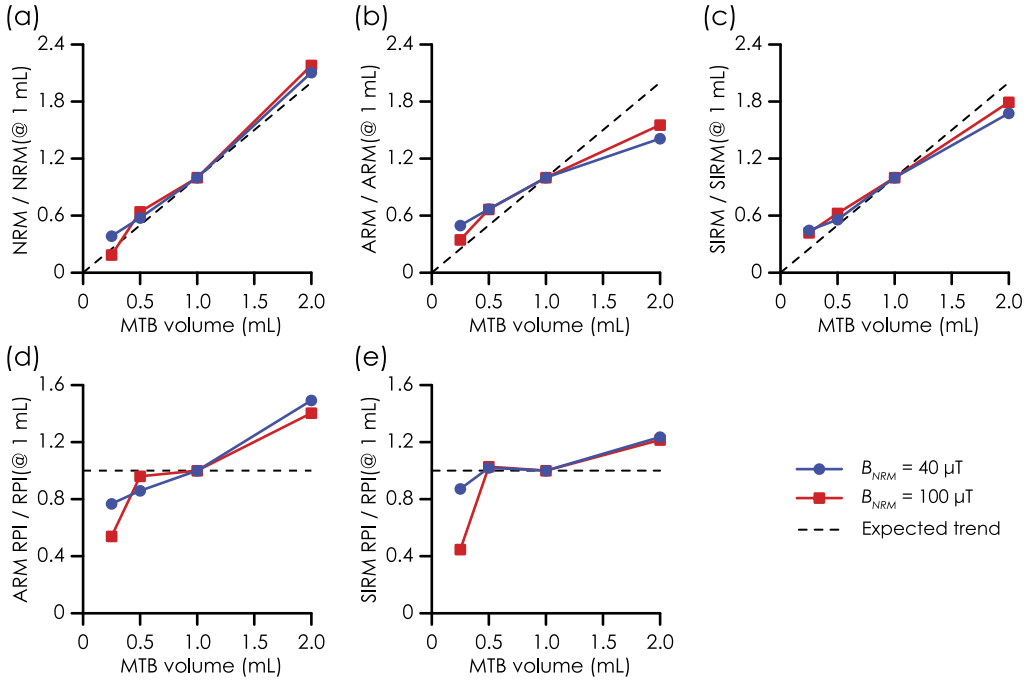

Fig. 7. The effects of varying the number the concentration of the initial solution on (a) NRM intensity, (b) ARM intensity, (c) SIRM intensity, (d) ARM normalized RPI, and (e) SIRM normalized RPI. Each data point is the average of two samples. In all cases the results have been normalized by the 1 mL volume results to allow comparison between the two B_{NRM} intensities investigated.

increase of ARM and SIRM with concentration, and the generally low χ_{ARM}/SIRM values, it is clear that magnetostatic interactions are influencing the acquisition of laboratory magnetizations. The width of a bacterial cell is often considered to be large enough to prevent three-dimensional interaction fields within an assemblage of MTB. Using numerical models of magnetically interacting crystals of magnetite, Muxworthy et al. (2003) demonstrated that interactions can have significant influence on SIRM at spacing equivalent to ~3 crystal diameters. A chain of magnetosomes effectively behaves like a single SD particle, for our average magnetosome size (~52 nm) and average magnetosomes per chain (~7), the average chain in our samples approximately corresponds to an equidimensional grain of ~100 nm. Therefore, the interaction distance for SIRM is up to ~0.3 μm. Egli (2006), however, demonstrated that at crystal spacing equivalent to less than ~28 crystal diameters was sufficient for interactions to have a noticeable effect on ARM. For our samples, this is equivalent to a distance of ~3 μm. For our AMB-1 samples, interactions may arise from two sources. First, interactions may arise between subchains within a single cell, which are separated by a distance of ~0.3 μm. Second, due to the non-disperse nature of our samples, inter-cell interactions (i.e., magnetosomes from one MTB cell interacting with magnetosomes from another MTB cell) may also be affecting ARM and SIRM acquisition. Importantly, while ARM and SIRM are likely influenced by magnetostatic interactions, these experiments indicate that the NRM acquisition process is completely unaffected by interactions. Our samples have a higher concentration of MTB than is typical for natural samples and should be more influenced than by magnetic interactions. The fact that the NRM of our samples behaves extremely well indicates that MTB in nature, that are not subject to post-depositional effects (e.g., dissolution), are likely to record the geomagnetic field well.

The increase of interactions is unlikely to be related to the disruption of the bacterial cells (i.e., the higher concentration samples have more disrupted cellular structures than the lower concentration samples). Each sample was prepared from the same culture and under the same conditions and therefore all samples should have experienced the same level of cell degradation. However, if differences in cell integrity were a factor this should manifest as low ARM ratios (e.g., Kobayashi et al., 2006) or as an increase in the full width at half maximum (FWHM) on the FORC diagram due to interactions (Chen et al., 2007; Li et al., 2012). FORC diagrams from representative samples with 2, 1, and 0.5 mL of bacterial solution are shown in Fig. 8 (the 0.25 mL samples were found to be too weak to measure). The FORC diagrams across a factor four increase in the number of MTB are near identical, which indicates that the cellular structure is intact.

ARM acquisition curves as a function of ARM bias field are shown in Fig. 9a. All of the samples lie approximately half way between the non-interacting (Kopp et al., 2006a) and interacting (Cisowski, 1981) extremes, which indicates moderate interactions for all samples (cf. Kobayashi et al., 2006; Kopp et al., 2006a, 2006b; Li et al., 2012). Although ARM acquisition systematically decreases with solution concentration for the 0.5, 1, and 2 mL samples there is considerable overlap between these data and the 0.25 mL samples yield a lower ARM acquisition curve than for the 0.5 and 1 mL samples. If we normalize the ARM acquisition curves by the volume of the MTB solution, which is a proxy for the relative number of MTB cells per sample, the expected trend emerges and the behaviour of the different samples becomes more distinct (Fig. 9b). The high scatter for the 0.25 mL samples may be due to a greater heterogeneity in the concentration of MTB for these samples. The overlap of behaviour seen in Fig. 9a is due to the fact that SIRM is also influenced by interactions in these samples (e.g., Fig. 7c).

The ARM ratio for the concentration samples is shown in Fig. 9c. As the concentration of the initial solution increases from 0.5 to 2 mL the ARM ratio decreases from 1.15 to 0.87×10^{-3} mA^{-1} (a ~25% decrease). These values are lower than for typical MTB (e.g., Moskowitz et al., 1993; Egli, 2004) and are a strong indication of increasing magnetic interactions within our samples (Egli, 2006). As noted above, heterogeneity in the concentration of the 0.25 mL solution likely yields the low ARM ratio measurement.

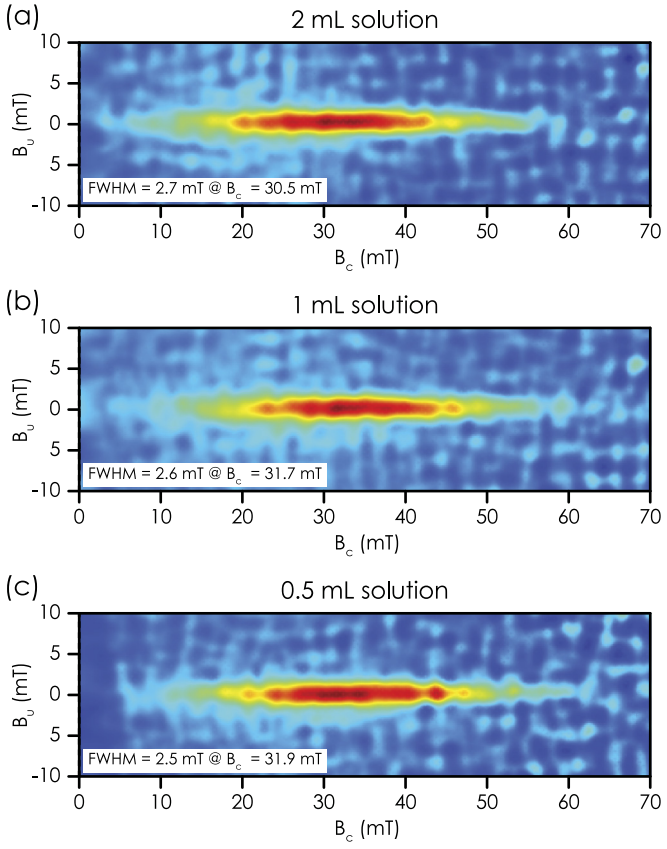

Fig. 8. FORC diagrams across a factor 4 variation in the concentration of the initial solution. In all diagrams $SF = 3$ ($\Delta B = 3.1$ mT). Diagrams have been obtained by averaging (a) 6, (b) 11, and (c) 15 FORC diagrams.

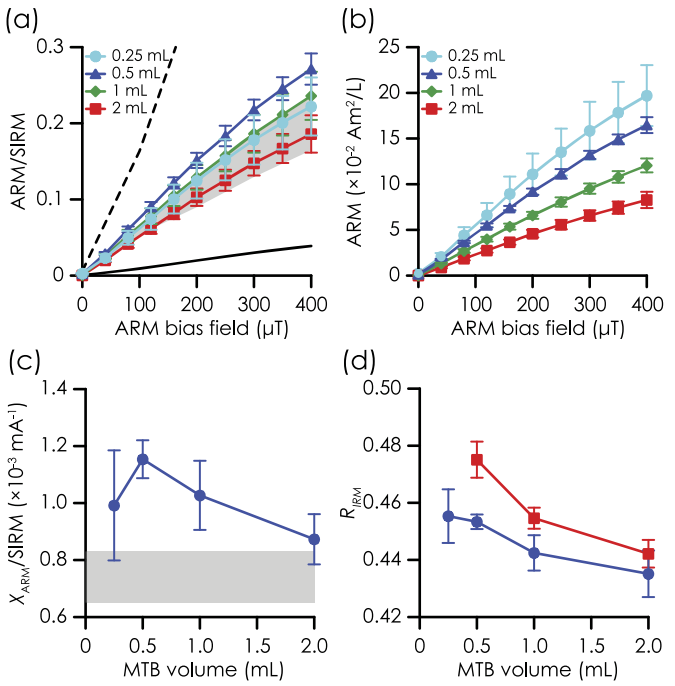

Fig. 9. (a) SIRM normalized ARM acquisition as a function of the bias field for the concentration samples. The black dashed line is the data from a mutant strain of *M. magneticum* (Kopp et al., 2006a), which represents the non-interacting case. The black solid line is the data from the highly interaction chiton tooth standard sample (Cisowski, 1981). (b) Volume normalized ARM acquisition as a function of the bias field. (c) Variation of χ_{ARM}/SIRM with concentration of the initial solution. (d) IRM and back-field demagnetization cross over point as a function of concentration as measured with the 2G pulse magnetizer (blue circles) and the VSM (red squares). In all plots the error bars represent ± one standard deviation. The grey shaded areas in parts a and c are the range of values (mean ± one standard deviation) obtained from the samples that yielded successful RPI estimates (Section 3.4). In part a, this is from 16 representative samples, in part b, it is from all 70 samples. (For interpretation of the references to color in this figure legend, the reader is referred to the web version of this article.)

The behaviour of the crossover point (R_{IRM}; Cisowski, 1981) between IRM acquisition and back-field demagnetization curves for the concentrations samples is shown in Fig. 9d. Pulse field data were measured on the 2G magnetometer and static field data on the VSM. Both measurements exhibit a systematic decrease of R_{IRM} with increasing solution concentration, which suggests an increase of magnetic interaction. For the static field data, the samples with the lowest concentration were too weak to clearly measure, but the 0.5 mL samples have an average R value of 0.475, which decreases to 0.442 for the 2 mL samples. The difference between these data and those from the gelatin capsule sample (Fig. 2) is most likely due to differences in sample preparation, specifically the drying time. The gelatin capsule sample was dried over $\lesssim$2 days, compared with the 5–6 days for the paleomagnetic samples. The more rapid drying time will minimize the shrinkage of the bacterial cells and maintain a larger inter-cellular chain spacing, which will minimize interactions.

The increase of interactions that we observe with increasing concentration of the initial solution is due to an increase in the strength of 3D interactions. As the number of MTB cells in each sample increases so does the depth of the final layer of dried sample. This should manifest as an increase of 3D interaction fields, which are stronger than the more 2D-like fields experienced by the lower concentration samples.

When compared with the FORC data, the above measured remanence data appear to be more sensitive to the interactions that are influencing the paleomagnetic data, in particular the ARM ratio, and highlight the discrepancy between in-field and remanence data. For our samples, we have closely packed MTB cells, which influences remanence data, but minimal cellular breakdown, hence little manifestation of interactions on the FORC diagrams. When considering natural samples, which may contain small amounts of multidomain particles and/or other interacting components, the influence of an interacting MTB component may be difficult to detect over and above these effects. Our ability to distinguish different interacting components in a complex system needs to be further investigated.

Given that the average subchain spacing in the MTB used for testing the linearity of NRM acquisition and RPI with applied field (Sections 3.3 and 3.4) will be the same as for the concentration samples, and that the inter-cellular packing may be similar, the samples that exhibit well behaved RPI data may also be influenced by magnetic interactions. The grey shaded area in shown Fig. 9a represents the range of ARM acquisition values (average ± one standard deviation) for 16 representative samples used in Fig. 5. These samples exhibit a degree of magnetic interactions comparable to the samples that were prepared with higher concentration solutions, but still yield reliable RPI estimates. For ARM normalized RPI, the 100 μT results are 2.4, 2.1, and 2.0 larger than the 40 μT results, for the 0.5, 1, and 2 mL solutions, respectively. This corresponds to an average of ~2.2 (±9%). For SIRM, the average increase is by a factor of 2.4 (±1%). The measured RPI increases from 40 μT to 100 μT shown Fig. 5 are factors of 2.2 and 2.3 for ARM and SIRM normalized RPI, respectively. Although only two field strengths were used for the samples with varying initial solution concentration, all of these increases compare well with the expected increase of a factor 2.5, which suggests that as long as the mean interaction field does not change between samples, RPI is recoverable, regardless of the presence of magnetic interactions.

The ARM ratio varies by ~10% between the different concentration samples, which implies that ARM ratio variations of <10% are needed to ensure that RPI estimates are unaffected by large variations magnetostatic interactions.

4.2. Implications for paleomagnetic records

Our SIRM values range from ~2–9 × 10^{-4} Am^2, which, if we assume our samples represent a standard paleomagnetic sample with a volume of 8 cm^3, corresponds to ~25–110 Am^{-1}. Both Dinarès-Turell et al. (2002) and Roberts et al. (2011) report IRM values on the order of 1–2 Am^{-1} for sediments dominated by MTB. Our samples are therefore likely to contain one to two orders of magnitude more MTB than natural samples. The basic alignment mechanism that these experiments simulate should be representative of the first-order behaviour of MTB in natural samples and although our samples are influenced magnetic interactions, which are likely to be much less for natural samples, natural MTB should record paleomagnetic signals in a fashion that is at least as good as what is simulated here (before consideration of other post-depositional processes, such as dissolution).

A key assumption in extracting relative paleointensity variations from sediments is that the NRM is linearly proportional to the field experienced during deposition and locking in of the magnetization. For the MTB studied here, NRM intensity is linear with deposition field, but does not exactly follow the expected trend, where a doubling of field strength is expected to result in a doubling of NRM intensity. Over the range of typical geomagnetic field intensities this deviation is small, and assuming a constant concentration of MTB, the maximum deviation of the RPI estimates from the true values will be no more than ~10–15% and will occur at the extreme highs and lows.

In Fig. 3c the NRM acquisition as function of applied field from our MTB experiments is compared to the detrital remanent magnetization (DRM) re-deposition experiments conducted by Johnson et al. (1948) and Spassov and Valet (2012). In this figure both the NRM and applied field strength have been normalized by the respective values at 40 μT for ease of comparison. For the Johnson et al. (1948) data, the original field strength data were scaled to the local geomagnetic field strength, which is taken to be 56.8 μT based on the DGRF for the laboratory location (Washington, DC, USA) in the mid-1940's. We have rescaled the data and interpolated the NRM intensity at 40 μT. From this comparison it can be seen that the deviation of our MTB experiments from the expected linear trend is comparable or less than the experiments using detrital material. There are, however, a number of significant differences between these three experiments in terms of the mechanisms being investigated. The Johnson et al. (1948) and Spassov and Valet (2012) experiments involved re-deposition of bulk sediment samples that simulated flocculation processes in a depositional environment. Due to low sedimentation rates, flocculation processes are unlikely to be significant in deep ocean sediments (e.g., Shcherbakov and Sycheva, 2010), where magnetofossils are commonly reported. Under such conditions, MTB will experience magnetic torques and alignment within sediment pore spaces and are likely to acquire magnetization in a fashion similar to post-deposition remanent magnetization (PDRM). Therefore, our results will be more representative post-depositional alignment experience by intact MTB cells and, to first order, should be akin to MTB alignment experienced in many natural environments.

MTB are found in broad range of depositional environments (e.g., Roberts et al., 2012; Bazylinski et al., 2013; Lin et al., 2013) and paleomagnetic records from these regions are likely to be a superimposition of PDRM alignment of MTB cells and processes influencing the remanence carried by the detrital component, which itself is likely to be a combination of DRM and PDRM mechanisms. The effect on such paleomagnetic records depends on the relative magnetization contributions of detrital and biogenically derived components. Given the linearity of the NRM with applied field from MTB, it seems more likely that any problems arising with mixing of biogenic and detrital magnetic particles may arise from the laboratory normalizations used and not in relation to how MTB acquire an NRM. One such potential source of discrepancy may arise from undetected magnetostatic interactions between bacterial and detrital magnetic components. Systematic study of these mixed environments is an important next step to fully understanding the influence that MTB and biogenically derived magnetic minerals have on paleomagnetic records.

One of the most important assumptions in relative paleointensity studies is that the chosen normalizer adequately accounts for variations in the concentration/amount of magnetic particles (Tauxe, 1993). Although our samples were not dispersed, they highlight the possibility of magnetic interactions that may influence paleomagnetic data, but that may go unrecognized in FORC diagrams. Remanence based proxies for magnetic interactions, such as the ARM ratio, are more useful tools for identifying the presence of paleomagnetically relevant magnetic interactions. The role and manifestation of magnetic interactions in sediments dominated by MTB needs to be further investigated, particularly in situations where MTB are mixed with detrital magnetic components.

This study has explored the first-order characteristics of magnetizations carried by MTB in a series of simplified depositional experiments. Many other factors, however, need to be investigated before we have a more complete picture of how MTB, and biogenically derived magnetic particles in general, influence paleomagnetic records. We have studied only a single cultured bacterial species, *M. magneticum* AMB-1. AMB-1 forms fragmental chains of magnetosomes, which are uncommon in wild MTB and these fragmental chains may enhance detrimental magnetic interactions (through subchain interactions). As discussed above, despite the presence of interactions, the paleomagnetic recordings are well behaved and natural MTB should record the field at least as good as AMB-1. In addition, in natural settings MTB are diverse and multiple species are frequently found coexisting in the same environment (e.g., Isambert et al., 2007; Moskowitz et al., 2008; Lin and Pan, 2009; Lin et al., 2013; Wang et al., 2013). Different MTB species have different magnetosome sizes and morphologies, compositions (magnetite and/or greigite), different chain structures (in terms of single versus multiple chains as well as magnetosome spacing), and widely differing numbers of magnetosomes per bacterial cell. All of these variations will manifest as differences in magnetic properties in terms of efficiency of alignment with the ambient magnetic field, demagnetization behaviour of NRM, ARM, and SIRM, as well as potential interaction fields, which we infer to be a limiting factor in ARM acquisition for our samples. Studies looking at a broad range of MTB species and developing an understanding of how MTB communities record the paleomagnetic field are therefore needed to develop a more general picture of how MTB manifest in paleomagnetic data.

5. Conclusions

The widespread abundance of magnetofossils in the geological record means that magnetic particles derived from MTB are significant contributors to paleomagnetic records. Although much work remains to be done, through simple deposition experiments, we have investigated the first-order characteristics of the fidelity and properties of paleomagnetic signals recorded by MTB.

The NRM recorded by our samples behaved extremely well and in a fashion that fits with expectations. Paleomagnetic directions are well constrained and lie close to the expected directions, which has been inferred from geological records dominated by MTB (e.g.,

Florindo and Roberts, 2005). The NRM acquired by MTB is near linear with applied field, such that over the range of typical geomagnetic field strengths (up to ~120 μT) the maximum deviations from the expected linear trend is no more than ~10%. For samples with similar numbers of bacterial cells, relative paleointensity estimates can be successfully recovered within the limits of the linearity of the NRM.

For our samples with variable amounts of bacterial cells, the effects of magnetic interactions on the paleomagnetic data are clearly observable. Although the NRM intensity increases with increasing MTB cells in the expected proportion, which is an indication that it is unaffected by interactions, both ARM and SIRM do not increase as expected. The relative increase of ARM with the number of MTB cells is less than for SIRM, which should be expected given that ARM is more sensitive to magnetic interactions. The widely held view that the bacterial cell shield magnetosome chains from inter-cellular magnetic interactions is likely not valid from the perspective of ARM and paleomagnetic analysis in our experiments where the MTB cell concentrations are high. The manifestation of interacting magnetosome chains may not be well represented by FORC diagrams and interaction estimates based on remanence behaviour may be more appropriate in paleomagnetic studies. As a result, magnetic interactions affecting paleomagnetic data may be more prevalent than realized and these effects need to be further investigated.

Acknowledgements

This work was funded by a State Key Laboratory of Lithospheric Evolution (IGGCAS) grant to G.A.P., the CAS/SAFEA International Partnership Program for Creative Research Teams (KZCX2-YW-T10) and NSFC grant (41240028) to Y.P. We thank Xiang Zhao for assistance with the Helmholtz coils and Fei Han and Xiaoqing He with bacteria preparation. Figs. 4c and 4d were produced using PmagPy v2.171 (Tauxe, 2010). We thank an anonymous reviewer for their suggestion and Ramon Egli for his thorough review and useful discussions.

References

Bazylinski, D.A., Frankel, R.B., 2004. Magnetosome formation in prokaryotes. Nat. Rev. Microbiol. 2, 217–230, http://dx.doi.org/10.1038/nrmicro842.

Bazylinski, D., Lefèvre, C., Schüler, D., 2013. Magnetotactic bacteria. In: Rosenberg, E., DeLong, E., Lory, S., Stackebrandt, E., Thompson, F. (Eds.), Magnetotactic Bacteria. Springer, Heidelberg, pp. 453–494.

Chang, S.-B.R., Kirschvink, J.L., Stolz, J.F., 1987. Biogenic magnetite as a primary remanence carrier in limestone deposits. Phys. Earth Planet. Inter. 46, 289–303, http://dx.doi.org/10.1016/0031-9201(87)90191-9.

Chen, A.P., Egli, R., Moskowitz, B.M., 2007. First-order reversal curve (FORC) diagrams of natural and cultured biogenic magnetic particles. J. Geophys. Res. 112, http://dx.doi.org/10.1029/2006jb004575. B08S90.

Cisowski, S., 1981. Interacting vs. non-interacting single domain behavior in natural and synthetic samples. Phys. Earth Planet. Inter. 26, 56–62, http://dx.doi.org/10.1016/0031-9201(81)90097-2.

Dinarès-Turell, J., Sagnotti, L., Roberts, A.P., 2002. Relative geomagnetic paleointensity from the Jaramillo Subchron to the Matuyama/Brunhes boundary as recorded in a Mediterranean piston core. Earth Planet. Sci. Lett. 194, 327–341, http://dx.doi.org/10.1016/S0012-821X(01)00563-5.

Efron, B., 1979. Bootstrap methods: Another look at the Jackknife. Ann. Stat. 7, 1–26, http://dx.doi.org/10.1214/aos/1176344552.

Egli, R., 2004. Characterization of individual rock magnetic components by analysis of remanence curves, 1. Unmixing natural sediments. Stud. Geophys. Geod. 48, 391–446, http://dx.doi.org/10.1023/B:SGEG.0000020839.45304.6d.

Egli, R., 2006. Theoretical considerations on the anhysteretic remanent magnetization of interacting particles with uniaxial anisotropy. J. Geophys. Res. 111, http://dx.doi.org/10.1029/2006jb004577. B12S18.

Egli, R., Chen, A.P., Winklhofer, M., Kodama, K.P., Horng, C.-S., 2010. Detection of noninteracting single domain particles using first-order reversal curve diagrams. Geochem. Geophys. Geosyst. 11, http://dx.doi.org/10.1029/2009gc002916. Q01Z11.

Florindo, F., Roberts, A.P., 2005. Eocene–Oligocene magnetobiochronology of ODP sites 689 and 690, Maud Rise, Weddell Sea, Antarctica. Geol. Soc. Am. Bull. 117, 46–66, http://dx.doi.org/10.1130/b25541.1.

Frankel, R.B., Blakemore, R.P., 1980. Navigational compass in magnetic bacteria. J. Magn. Magn. Mater. 15–18, 1562–1564, http://dx.doi.org/10.1016/0304-8853(80)90409-6.

Guyodo, Y., Valet, J.-P., 1996. Relative variations in geomagnetic intensity from sedimentary records: The past 200,000 years. Earth Planet. Sci. Lett. 143, 23–36, http://dx.doi.org/10.1016/0012-821X(96)00121-5.

Hanzlik, M., Winklhofer, M., Petersen, N., 1996. Spatial arrangement of chains of magnetosomes in magnetotactic bacteria. Earth Planet. Sci. Lett. 145, 125–134, http://dx.doi.org/10.1016/S0012-821X(96)00191-4.

Harrison, R.J., Feinberg, J.M., 2008. FORCinel: An improved algorithm for calculating first-order reversal curve distributions using locally weighted regression smoothing. Geochem. Geophys. Geosyst. 9, http://dx.doi.org/10.1029/2008GC001987. Q05016.

Heslop, D., Roberts, A.P., 2012. Estimation of significance levels and confidence intervals for first-order reversal curve distributions. Geochem. Geophys. Geosyst. 13, http://dx.doi.org/10.1029/2012gc004115. Q12Z40.

Isambert, A., Menguy, N., Larquet, E., Guyot, F., Valet, J.-P., 2007. Transmission electron microscopy study of magnetites in a freshwater population of magnetotactic bacteria. Am. Mineral. 92, 621–630, http://dx.doi.org/10.2138/am.2007.2278.

Johnson, E.A., Murphy, T., Torreson, O.W., 1948. Pre-history of the Earth's magnetic field. Terr. Magn. Atmos. Electr. 53, 349–372, http://dx.doi.org/10.1029/TE053i004p00349.

King, J.W., Banerjee, S.K., Marvin, J., 1983. A new rock-magnetic approach to selecting sediments for geomagnetic paleointensity studies: Application to paleointensity for the last 4000 years. J. Geophys. Res. 88, 5911–5921, http://dx.doi.org/10.1029/JB088iB07p05911.

Kirschvink, J.L., 1980. The least-squares line and plane and the analysis of palaeomagnetic data. Geophys. J. R. Astron. Soc. 62, 699–718, http://dx.doi.org/10.1111/j.1365-246X.1980.tb02601.x.

Kirschvink, J.L., 1982. Paleomagnetic evidence for fossil biogenic magnetite in western Crete. Earth Planet. Sci. Lett. 59, 388–392, http://dx.doi.org/10.1016/0012-821X(82)90140-6.

Kobayashi, A., Kirschvink, J.L., Nash, C.Z., Kopp, R.E., Sauer, D.A., Bertani, L.E., Voorhout, W.F., Taguchi, T., 2006. Experimental observation of magnetosome chain collapse in magnetotactic bacteria: Sedimentological, paleomagnetic, and evolutionary implications. Earth Planet. Sci. Lett. 245, 538–550, http://dx.doi.org/10.1016/j.epsl.2006.03.041.

Kopp, R.E., Kirschvink, J.L., 2008. The identification and biogeochemical interpretation of fossil magnetotactic bacteria. Earth-Sci. Rev. 86, 42–61, http://dx.doi.org/10.1016/j.earscirev.2007.08.001.

Kopp, R.E., Nash, C.Z., Kobayashi, A., Weiss, B.P., Bazylinski, D.A., Kirschvink, J.L., 2006a. Ferromagnetic resonance spectroscopy for assessment of magnetic anisotropy and magnetostatic interactions: A case study of mutant magnetotactic bacteria. J. Geophys. Res. 111, http://dx.doi.org/10.1029/2006jb004529. B12S25.

Kopp, R.E., Weiss, B.P., Maloof, A.C., Vali, H., Nash, C.Z., Kirschvink, J.L., 2006b. Chains, clumps, and strings: Magnetofossil taphonomy with ferromagnetic resonance spectroscopy. Earth Planet. Sci. Lett. 247, 10–25, http://dx.doi.org/10.1016/j.epsl.2006.05.001.

Korte, M., Constable, C.G., 2005. Continuous geomagnetic field models for the past 7 millennia: 2. CALS7K. Geochem. Geophys. Geosyst. 6, Q02H16, http://dx.doi.org/10.1029/2004GC000801.

Larrasoaña, J.C., Roberts, A.P., Rohling, E.J., 2008. Magnetic susceptibility of eastern Mediterranean marine sediments as a proxy for Saharan dust supply?. Mar. Geol. 254, 224–229, http://dx.doi.org/10.1016/j.margeo.2008.06.003.

Li, J., Pan, Y., Chen, G., Liu, Q., Tian, L., Lin, W., 2009. Magnetite magnetosome and fragmental chain formation of Magnetospirillum magneticum AMB-1: transmission electron microscopy and magnetic observations. Geophys. J. Int. 177, 33–42, http://dx.doi.org/10.1111/j.1365-246X.2009.04043.x.

Li, J., Wu, W., Liu, Q., Pan, Y., 2012. Magnetic anisotropy, magnetostatic interactions and identification of magnetofossils. Geochem. Geophys. Geosyst. 13, http://dx.doi.org/10.1029/2012gc004384. Q10Z51.

Lin, W., Pan, Y., 2009. Uncultivated magnetotactic cocci from Yuandadu Park in Beijing, China. Appl. Environ. Microbiol. 75, 4046–4052, http://dx.doi.org/10.1128/aem.00247-09.

Lin, W., Li, J., Pan, Y., 2012. Newly isolated but uncultivated magnetotactic bacterium of the phylum Nitrospirae from Beijing, China. Appl. Environ. Microbiol. 78, 668–675, http://dx.doi.org/10.1128/aem.06764-11.

Lin, W., Wang, Y., Gorby, Y., Naealson, K., Pan, Y., 2013. Integrating niche-based process and spatial process in biogeography of magnetotactic bacteria. Sci. Rep. 3, 1643, http://dx.doi.org/10.1038/srep01643.

Moskowitz, B.M., Frankel, R.B., Bazylinski, D.A., 1993. Rock magnetic criteria for the detection of biogenic magnetite. Earth Planet. Sci. Lett. 120, 283–300, http://dx.doi.org/10.1016/0012-821X(93)90245-5.

Moskowitz, B.M., Bazylinski, D.A., Egli, R., Frankel, R.B., Edwards, K.J., 2008. Magnetic properties of marine magnetotactic bacteria in a seasonally stratified coastal pond (Salt Pond, MA, USA). Geophys. J. Int. 174, 75–92, http://dx.doi.org/10.1111/j.1365-246X.2008.03789.x.

Muxworthy, A.R., Williams, W., 2006. Critical single-domain/multidomain grain sizes in noninteracting and interacting elongated magnetite particles: Implications for magnetosomes. J. Geophys. Res. 111, http://dx.doi.org/10.1029/2006jb004588. B12S12.

Muxworthy, A.R., Williams, W., 2009. Critical superparamagnetic/single-domain grain sizes in interacting magnetite particles: implications for magnetosome crystals. J. R. Soc. Interface 6, 1207–1212, http://dx.doi.org/10.1098/rsif.2008.0462.

Muxworthy, A., Williams, W., Virdee, D., 2003. Effect of magnetostatic interactions on the hysteresis parameters of single-domain and pseudo-single-domain grains. J. Geophys. Res. 108, 2517, http://dx.doi.org/10.1029/2003jb002588.

Pan, Y., Petersen, N., Davila, A.F., Zhang, L., Winklhofer, M., Liu, Q., Hanzlik, M., Zhu, R., 2005. The detection of bacterial magnetite in recent sediments of Lake Chiemsee (southern Germany). Earth Planet. Sci. Lett. 232, 109–123, http://dx.doi.org/10.1016/j.epsl.2005.01.006.

Petersen, N., von Dobeneck, T., Vali, H., 1986. Fossil bacterial magnetite in deep-sea sediments from the South Atlantic Ocean. Nature 320, 611–615, http://dx.doi.org/10.1038/320611a0.

Pike, C.R., Roberts, A.P., Verosub, K.L., 1999. Characterizing interactions in fine magnetic particle systems using first order reversal curves. J. Appl. Phys. 85, 6660–6667, http://dx.doi.org/10.1063/1.370176.

Roberts, A.P., Pike, C.R., Verosub, K.L., 2000. First-order reversal curve diagrams: A new tool for characterizing the magnetic properties of natural samples. J. Geophys. Res. 105, 28461–28475, http://dx.doi.org/10.1029/2000JB900326.

Roberts, A.P., Florindo, F., Villa, G., Chang, L., Jovane, L., Bohaty, S.M., Larrasoaña, J.C., Heslop, D., Fitz Gerald, J.D., 2011. Magnetotactic bacterial abundance in pelagic marine environments is limited by organic carbon flux and availability of dissolved iron. Earth Planet. Sci. Lett. 310, 441–452, http://dx.doi.org/10.1016/j.epsl.2011.08.011.

Roberts, A.P., Chang, L., Heslop, D., Florindo, F., Larrasoaña, J.C., 2012. Searching for single domain magnetite in the “pseudo-single-domain” sedimentary haystack: Implications of biogenic magnetite preservation for sediment magnetism and relative paleointensity determinations. J. Geophys. Res. 117, http://dx.doi.org/10.1029/2012jb009412. B08104.

Shcherbakov, V., Sycheva, N., 2010. On the mechanism of formation of depositional remanent magnetization. Geochem. Geophys. Geosyst. 11, http://dx.doi.org/10.1029/2009gc002830. Q02Z13.

Spassov, S., Valet, J.-P., 2012. Detrital magnetizations from redeposition experiments of different natural sediments. Earth Planet. Sci. Lett. 351–352, 147–157, http://dx.doi.org/10.1016/j.epsl.2012.07.016.

Stolz, J.F., Chang, S.-B.R., Kirschvink, J.L., 1986. Magnetotactic bacteria and single-domain magnetite in hemipelagic sediments. Nature 321, 849–851, http://dx.doi.org/10.1038/321849a0.

Tarduno, J.A., Tian, W., Wilkison, S., 1998. Biogeochemical remanent magnetization in pelagic sediments of the western equatorial Pacific Ocean. Geophys. Res. Lett. 25, 3987–3990, http://dx.doi.org/10.1029/1998gl900079.

Tauxe, L., 1993. Sedimentary records of relative paleointensity of the geomagnetic field: Theory and practice. Rev. Geophys. 31, 319–354, http://dx.doi.org/10.1029/93rg01771.

Tauxe, L., 2010. Essentials of Paleomagnetism. University of California Press, Berkeley.

Tauxe, L., Pick, T., Kok, Y.S., 1995. Relative paleointensity in sediments: A pseudo-Thellier approach. Geophys. Res. Lett. 22, 2885–2888, http://dx.doi.org/10.1029/95GL03166.

Tauxe, L., Gee, J.S., Staudigel, H., 1998. Flow directions in dikes from anisotropy of magnetic susceptibility data: The bootstrap way. J. Geophys. Res. 103, 17775–17790, http://dx.doi.org/10.1029/98jb01077.

Wang, Y., Lin, W., Li, J., Pan, Y., 2013. High diversity of magnetotactic deltaproteobacteria in a freshwater niche. Appl. Environ. Microbiol. 79, 2813–2817, http://dx.doi.org/10.1128/aem.03635-12.

Yamazaki, T., Yamamoto, Y., Acton, G., Guidry, E.P., Richter, C., 2013. Rock-magnetic artifacts on long-term relative paleointensity variations in sediments. Geochem. Geophys. Geosyst., 29–43, http://dx.doi.org/10.1029/2012gc004546.